VI International Conference on Computational Methods for Coupled Problems in Science and Engineering
COUPLED PROBLEMS 2015
B. Schrefler, E. Oñate and M. Papadrakakis(Eds)

A COMPUTATIONAL MULTISCALE APPROACH TO COUPLE HYGRO-MECHANICAL RESPONSES OF LARGE-SCALE MASONRY WALLS

G. CASTELLAZZI*, S. de MIRANDA*, G. FORMICA†, L. MOLARI* AND F. UBERTINI*

*DICAM Department
University of Bologna
Viale del Risorgimento 2, 40136 Bologna, Italy
Web page: http://www.eng.dicam.unibo.it

†Dipartimento di Architettura
Università degli Studi "Roma Tre"
via della Madonna dei Monti 40, 00184 Roma, Italy
e-mail: formica@uniroma3.it, web page: http:/http://host.uniroma3.it/docenti/formica

Key words: Computational Multiscale approach, mechanical and environmental coupled degradations.

Abstract. We present a computational multiscale approach to the nonlinear problems of humidity diffusion and mechanical damage of large-scale masonry walls, and their coupling in terms of the effects of the humidity diffusion on the mechanical response and the effects of the mechanical degradation on the diffusion process. Such an approach allows us to recover, both efficiently and accurately, the complex nonlinear response of large-scale walls, which are in general hard to be solved by means of standard numerical tools.
Two representative tests of two- and three-storey walls are here analyzed, and the corresponding results reported and commented, aiming to show how samples like these can potentially serve as reference solutions for more applicative purposes.

1 INTRODUCTION

The models of the two nonlinear problems, humidity diffusion and structural equilibrium, consider the wall as a lattice-like discrete system [1, 2], where the field variables are associated to each block composing the wall, i.e. sandstone units, while the nonlinear response is assumed to be concentrated at interface elements, i.e. cement mortar joints. Although such models drastically simplify the corresponding physical phenomena, or more sophisticated models [3], they present all the relevant nonlinearities of the problems, such as the water uptake process under evaporation conditions, and the structural frictional

toughness along with the softening material response. In order to address to more realistic structural contexts, large-scale walls are hard to be solved numerically, even working with physical models as simplified as the discrete models here adopted [1]. Regardless of the computational costs which increase with the number of blocks in the masonry texture, the nonlinearities of the physical problems can lead to difficulties in convergence [4]. Such nonlinearities and consequent failures in convergence are essentially related to localization phenomena of the physical responses: roughly speaking, the water uptake process tends to concentrate the humidity distribution in sharp fronts, in reason of the simultaneous evaporation process; on the other hand, the strain localizes and produces mechanical damage, so that the wall stress response becomes softening.

Following the approach proposed in [5] for pure mechanical contexts and then extended to the diffusive context in [2], the discrete systems are solved by an iterative multilevel strategy mimicking algebraic multigrid methods, where local solutions, those of balancing between two linked blocks, and global solutions, those of balancing two contiguous patterns of blocks, work as nested sequences able to correct error distributions with high and low frequency oscillation, respectively.

We conduct a numerical testing, whose meaningful results are here reported. We essentially show how the diffusion properties are affected by existing damage patterns in equilibrium with certain loading conditions, and conversely, how strength and elastic properties are degraded by existing distributions of humidity through water uptake processes in steady-state. In particular, the results obtained on a two- and a three-storey wall are discussed and compared.

2 COMPUTATIONAL MULTISCALE APPROACH

2.1 A sketch of the hygro-mechanical model

Here we summarize modelling equations of both diffusive and mechanical problems, first proposed and validated in [2] and [1], respectively. The two physical problems are both modelled in a 2D context basing on a Lagrangean formulation which leads to describe the wall as a lattice-like discrete system.

Each brick is ideally divided in two blocks, where both humidity and displacement variable fields are described by discrete parameters which refer to the block centroid: one parameter generalizes the humidity scalar field over the block, while the kinematics vector field is generalized in terms of three parameters, namely two displacement components and the rotation of the block. Each block interacts with the n surrounding blocks through the corresponding (two bed plus two head) mortar joints (n is equal to 3 or 4, depending on whether the block is at the boundary or not). Such interactions are governed by constitutive prescriptions which allow us to model each mortar joint as an interface exhibiting the nonlinear response of both physical problems; in particular, the interface corresponding to one of the two head joints accounts for the nonlinear response that develops within the single real brick. Figure 1 sketches the key-points building up the discrete model:

(a) initial 3D model to be discretized; (b) 2D discrete model; (c) the block as physical Representative Elementary Volume (REV); kinematical (d) and humidity (g) descriptors; interface nonlinear responses in terms of stresses (e) and moisture flux (h), and corresponding tangent mechanical stiffness (f) and diffusive permeability (i) of the interfaces depicted as springs.

Referring to Figure 1 for definitions of geometrical and physical symbols, and denoting with h_i and $h_{(k)}$ the values of the humidity h at the centroids of the i-th block and of the k-th surrounding block, the discrete moisture-balance equation of each block reads as:

$$\overline{c}_{w,h}[h_i]\frac{\partial h_i}{\partial t} + \frac{1}{\Omega_b}\sum_{k=1}^{n}\frac{b_{(k)}}{l_{(k)}}\overline{C}_h[h_{(k)}]\Big(h_{(k)} - h_i\Big) - \overline{\gamma}_w[h_i]\Big(h_i - h_{\text{env}}\Big) = 0 \tag{1}$$

where barred quantities mean that the corresponding continuum quantities are homogenized over the REV, according to an averaging procedure of material and geometric properties of bricks and joints involved in the same REV. In particular, $\overline{c}_{w,h}$ is the equivalent ratio of moisture content c_w, $\overline{C}_{h(k)}$ is the equivalent interface permeability between two blocks, and $\overline{\gamma}_w$ is the humidity convective term accounting for the evaporation conditions across the wall thickness. Finally, h_{env} is the prescribed environmental humidity. Further details can be found in [3, 2].

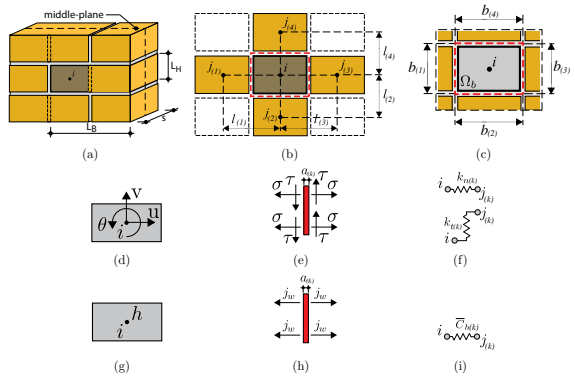

Figure 1: Representation of the generation of the discrete model.

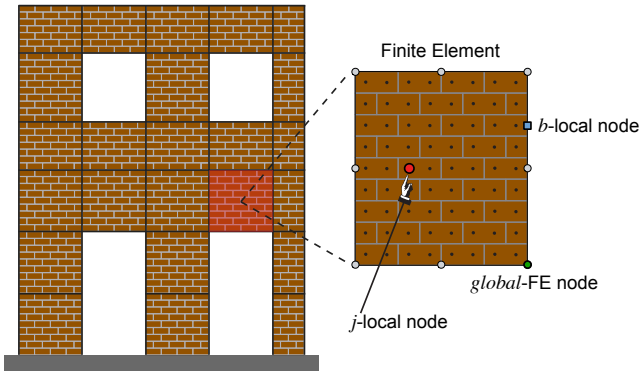

Figure 2: Representation of the different scales/levels.

The discrete equilibrium equations of each block are generated similarly: the second term in (1) assembles in the same way the stress contributions through the interfaces surrounding the block, while the last source term in (1) corresponds in the mechanical problem to possible loads referred to the block centroid; the first ratio-dependent term is instead not present. The equivalent, normal and shear, stress contributions (σ, τ) across the interfaces depend nonlinearly on the differential displacements (ε, γ) of the surrounding blocks with respect to each considered block [1]:

$$\sigma = \frac{k_{n(k)}\,\varepsilon}{1+\alpha_{(k)}H(\varepsilon)}\,, \qquad \tau = \frac{k_{t(k)}\gamma\left\{1+\alpha_{(k)}[1-H(\varepsilon)]\right\} - \alpha_{(k)}\overline{\tau}_{(k)}H(-\varepsilon)}{1+\alpha_{(k)}}. \tag{2}$$

In (2), $k_{n(k)}$ and $k_{t(k)}$ are, respectively, the normal and tangential stiffness associated to the k-th joint, $\alpha_{(k)}$ is the damage parameter of the k-th joint, and $\overline{\tau}_{(k)}$ is the frictional toughness equivalent to a fully-damaged joint. $\overline{\tau}_{(k)}$ obeys to the Coulomb criterion:

$$\overline{\tau}_{(k)} = k_{t(k)}\gamma - \max\left\{-\mu_{(k)}\sigma,\, \min[\mu_{(k)}\sigma,\, \tau_{0(k)} + k_{t(k)}(\gamma - \gamma_0)]\right\}, \tag{3}$$

being $\mu_{(k)}$ the friction coefficient of the mortar/brick interface, and $\tau_{0(k)}$ and γ_0 the current values of $\tau_{(k)}$ and γ. Moreover, H is the Heaviside function, so as to switch compressive to tensile conditions of the joint. Therefore, in compression the joint behaves as linearly elastic, except for a Coulomb frictional toughness $\overline{\tau}_{(k)}$.

2.2 Numerical strategy

The two analyses of humidity diffusion and mechanical response run separately, the former requiring a time-integration solution, the latter a parametric solution in the shear-load amplification factor. In particular, for the humidity diffusion problem we use the generalized-alpha method, as defined in [6]; a path-following technique recovers the pseudo-static equilibrium paths of the mechanical problem, according to the scheme first proposed in [1] and then developed in [5].

The two physics are coupled just in the initialization phase of the processes, where the material diffusion parameters are modified in dependence on a known damage pattern, and the material mechanical coefficients in dependence on a given humidity distribution. From a computational point of view, both analyses require iterative solvers which actually reveal the same complexity, sharing several parts of the algorithmic frameworks.

Indeed, both the iterative solution schemes solve the linearized problem serving as corrector step of an initial guess. Let $\boldsymbol{u}_l$ be the vector of initial guess: $\boldsymbol{u}_l$ collects the discrete parameters that correspond to the values of humidity of all the sandstone blocks, in a case, and the displacements of all the sandstone blocks, in the other case. The corrector step within the iterative strategies solves the following residual problem:

$$\boldsymbol{r}_l\left[\delta\boldsymbol{u}_l\right] = \boldsymbol{f}_l - \boldsymbol{s}\left[\delta\boldsymbol{u}_l\right] = \boldsymbol{0}\,, \quad \text{with } \boldsymbol{s}\left[\delta\boldsymbol{u}_l\right] = \boldsymbol{K}\left[\boldsymbol{u}_l\right]\delta\boldsymbol{u}_l \tag{4}$$

where $\boldsymbol{r}_l$ is the residue, $\boldsymbol{f}_l$ is the known term, and $\boldsymbol{s}\left[\delta\boldsymbol{u}_l\right]$ is the linearized physical response: $\boldsymbol{K}\left[\boldsymbol{u}_l\right]$ is the tangent matrix of the problem computed at the current solution $\boldsymbol{u}_l$, and $\delta\boldsymbol{u}_l$ is the correction variable to find that updates $\boldsymbol{u}_l$; $\boldsymbol{K}\left[\boldsymbol{u}_l\right]$ serves as iteration matrix.

As proved in [5] and then in [2], computational multiscale approaches can successfully avoid problems in convergence occurring when analyzing nonlinear responses of large-scale walls. We distinguish two scales of representation (see Figure 2), i.e. the (reference) *local* scale, defined at each block by the discrete models, and the *global* scale, defined as Finite Elements which are a representation of the same local problems for a certain pattern of blocks. Within an iterative scheme that reaches convergence at the reference scale, the two scales serve both as partial solutions of the whole problem: the global scale is used as a pre-conditioner of the local scale and corrects smooth distributions of the iterative

error, while the local scale is used to solve the interaction between two blocks at a time and then corrects high-frequency oscillations of distribution of the error.

Introducing for vectors and matrices subscripts l and g to label local and global quantities, respectively, the global-level sequence of algorithmic operations starts from a trial solution $\boldsymbol{u}_l$ affected by the error $\boldsymbol{r}_l$, and consists of the following solutions:

$$\boldsymbol{r}_g = \boldsymbol{A}^\top \boldsymbol{r}_l \quad \Rightarrow \quad \boldsymbol{d}_g = \boldsymbol{K}_g^{-1} \boldsymbol{r}_g \quad \Rightarrow \quad \boldsymbol{u}_l^{\text{new}} = \boldsymbol{u}_l + \boldsymbol{A}\boldsymbol{d}_g \tag{5}$$

In such a sequence, the first and latter items use the so-called scale bridging operator $\boldsymbol{A}$, to perform local-to-global and global-to-local transformations, respectively: in particular, $\boldsymbol{A}^\top$ works as restriction of the local error to the global (coarser) error, while $\boldsymbol{A}$ interpolate the global correction into a (finer) local correction which update the initial local solution. Since this updated solution is usually affected by a new, high frequency, error $\boldsymbol{r}_l$, a smoothing process works at local level, according to the following equations:

$$\boldsymbol{d}_l = \boldsymbol{K}_l^{-1} \boldsymbol{r}_l \quad \Rightarrow \quad \boldsymbol{u}_l^{\text{new}} = \boldsymbol{u}_l + \boldsymbol{d}_l \tag{6}$$

Note that the local-level iteration (6) is enabled on the basis of a threshold criterion, which is imposed on the global error e_g left by the global-level solutions (5); on the other hand, the global level can run when the local error e_l, resulting from local-level corrections, reduce by a factor $c < 1$ the global error e_g, ie. $e_l < c\, e_g$.

The key-role is actually ruled by the scale bridging operator $\boldsymbol{A}$, which is derived numerically for each Finite Element simultaneously. The algorithm, implementing a sort of algebraic homogenization procedure, results from a linearized solution computed at the level of the single element: in one stage the linearized balance equations are solved in terms of the discrete variables of the blocks surrounding the element boundary; these boundary variables are then imposed to be perfectly conform to the shape functions describing the same variables in terms of the element at the global scale. This way to proceed minimizes the numerical error introduced while smoothing the local evaluation of the variables. Besides, it allows us to derive the global tangent matrix $\boldsymbol{K}_g$, which turns out to be the best coarse representation of the (finer) tangent matrix of the local problem $\boldsymbol{K}[\boldsymbol{u}_l]$ when the local problem is linear [4].

Consider the local linearized balance, which represents a general form valid for both the mechanical and the diffusive solution scheme, as the following system,

$$\begin{bmatrix} \boldsymbol{K}_l^{jj} & \boldsymbol{K}_l^{jb} \\ \left(\boldsymbol{K}_l^{jb}\right)^\top & \boldsymbol{K}_l^{bb} \end{bmatrix} \begin{bmatrix} \boldsymbol{d}_l^j \\ \boldsymbol{d}_l^b \end{bmatrix} = \begin{bmatrix} \boldsymbol{r}_l^j \\ \boldsymbol{r}_l^b \end{bmatrix}. \tag{7}$$

Here we assume a local linearized balance for each Finite Element, i.e. the global scale, containing a certain pattern of bricks, which, in turn, contains the local scale, separating brick local variables internal to the Element (labeled with superscript j) from those at the boundary of the same Element (labeled with superscript b), see Figure 2. The Finite Element size is defined by the user and, of course, must be a multiple of the brick size.

Therefore, solving by condensation in the local problem (7) the internal variables $\boldsymbol{d}_l^j$ in terms of the boundary variables $\boldsymbol{d}_l^b$, and enforcing $\boldsymbol{d}_l^b$ to be exactly conform to the interpolation used to define the Finite Element representing the global scale, i.e. $\boldsymbol{d}_l^b = \boldsymbol{N}\boldsymbol{d}_g$, we finally obtain the scale bridging matrix for the generic Element as

$$\boldsymbol{A} = \left(\boldsymbol{K}_l^{jj}\right)^{-1}\boldsymbol{K}_l^{jb}\boldsymbol{N}, \tag{8}$$

where $\boldsymbol{N}$ is the matrix collecting the shape functions of each Element, evaluated at the centroids of the boundary bricks. In particular, a 8-node Serendipity interpolation is used as shape functions.
The global tangent matrix is then picked up by the remaining internal variables of the same local problem (7): by imposing a mutual work identity between the two scales, i.e. $\boldsymbol{r}_l^\top \boldsymbol{d}_l = \boldsymbol{r}_g^\top \boldsymbol{d}_g$, for each Element we have

$$\boldsymbol{K}_g = \boldsymbol{N}^\top \left[\left(\boldsymbol{K}_l^{bb}\right)^{-1} - \left(\boldsymbol{K}_l^{jb}\right)^\top \left(\boldsymbol{K}_l^{jj}\right)^{-1}\boldsymbol{K}_l^{jb}\right]\boldsymbol{N}. \tag{9}$$

Each Element is therefore balanced internally, i.e. the local linearized balance problem is satisfied at each element separately, while it is compatible along its boundary with a local solution. It means that if the local solution is exactly the one predicted by the interpolating Serendipity functions at each Element boundary, then the global level reach the exact linearized solution everywhere. As concerns $\boldsymbol{K}_l$, since it has to be able to correct local fluctuations of the error, it corresponds to the tangent matrix of the problem defined at a single block. Thus, the correction of the local variables is made block by block, regardless of the influence of the blocks surrounding it, as well as a Gauss-Seidel iterative scheme.

3 NUMERICAL RESULTS

The validation of the discrete model in terms of pure mechanical response has been carried out in [5], considering applications at the structural scale as well. The validation of the discrete diffusive model has been made in [2] by comparing the two-dimensional discrete model with the three-dimensional continuum diffusive model, already proposed and tuned on experimental evidences in [3].

In this section the proposed numerical strategy is applied to two significant large-scale walls, characterized by different aspect ratios (height-over-width) of the wall size: the former about 1, the latter about 3/2. Two masonry walls of two and three storeys respectively were tested, whose geometries are depicted in Figure 3.
For both the walls we report: i) equilibrium curves providing shear-load carrying capacity, see Figure 4; ii) uptake curves, measuring the cumulative volumetric water inflow up to steady-state conditions, see Figure 5; iii) damage maps depicting in white-to-red color scale joints with different values of damage (red color to 100% damaged joints), overlapped with humidity maps depicting in white-to-aqua scale blocks with different values of water content (aqua color to 100% wet blocks), see Figures 6 and 7 .

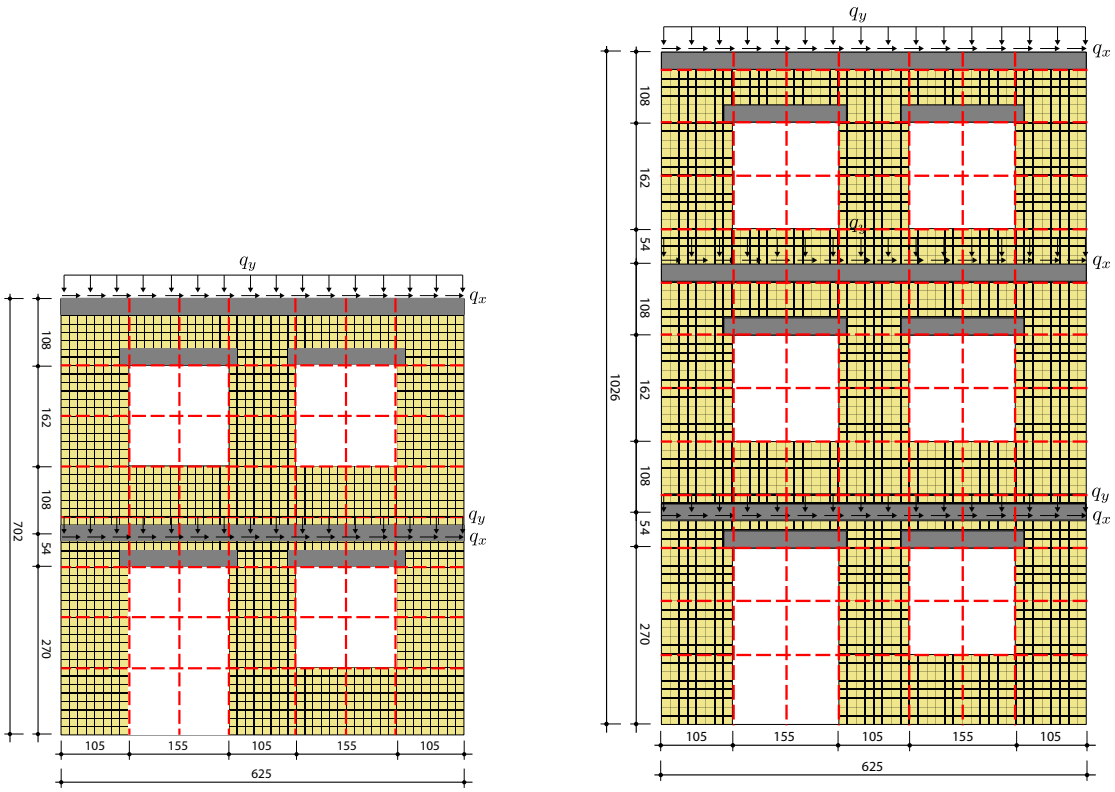

(a) Two-storey wall (b) Three-storey wall

Figure 3: Geometry of the tested walls (units in centimetres). FE mesh in red dashed lines.

3.1 Material properties and coupling relationships

Isothermal conditions are assumed, with the temperature $T = 293K$. The material properties of the sandstone and cement mortar come from various experimental evidences (see [1]–[5] for further details and references), and they are listed in Table 1. Note that we adopt the following empirical expressions, as proposed in [7], for adsorption isotherm and for liquid conductivity:

$$c_w = \phi\rho_w \frac{\psi - 1}{\psi - h} h\,, \quad K_l = 3.8 \left(\frac{A}{\phi\rho_w}\right)^2 10^{3(S_w - 1)} \frac{\partial c_w}{\partial h} \frac{h}{\rho_w R_v T}, \tag{10}$$

where A is the water adsorption coefficient, R_v the gas constant of water vapour, ρ_w the water density, and the parameter $\psi = 0.8 \dfrac{c_{w80} - \phi\rho_w^l}{c_{w80} - \phi\rho_w^l 0.8}$ fits the experimental data by enforcing the measured value of water content at relative humidity $h = 0.8$.

The coupling phenomena are here modelled by constitutive relationships investing key material quantities: i) the sandstone elastic (Young) modulus and the mortar tensile strength, both decreasing as the water saturation degree increases; ii) the mortar perme-

Table 1: Material property parameters.

meule sandstone	parameter	cement mortar
$A = 0.225$	water adsorption [kg/m^2/s$^{1/2}$]	$A = 0.015$
$\phi = 0.235$	porosity	$\phi = 0.23$
$\rho = 2077$	density [kg/m^3]	$\rho = 2053$
$c_{w80} = 8.31$	water content at $h = 0.8$ [kg/m^3]	$c_{w80} = 59.3$
$\frac{D_v}{R_v T} = 4.401\text{e-}11$	vapour permeability [kg/s/Pa/m]	$\frac{D_v}{R_v T} = 1.965\text{e-}11$
$E = 19$	Young's modulus [GPa]	$E = 0.5$
$G = 3.8$	tangential modulus [GPa]	$G = 0.1$
$\sigma_t = 40$	tensile strength [MPa]	$\sigma_t = 21$
$\mu = 0.467$	friction coefficient	$\mu = 0.467$

ability which increases as the mechanical damage increases.
The former relationships rule how mechanical characteristics are affected by the presence of humidity in the wall, and they are expressed in terms of the water saturation degree $S_w = c_w \big/ \rho_w \phi$. The sandstone elastic modulus obeys to the following law

$$E = 3.121 + 19.06 \Big/ S_w 100 \text{ [GPa]} \tag{11}$$

according to experimental results reported and interpreted in [8]. On the basis of the same work, the decay law of the cement tensile strength was derived and proposed in [2]:

$$\sigma_t = -7 \left((S_w - 10) \big/ 100 \right)^{1/5} + 21 \text{ [MPa]} \tag{12}$$

Such a law is valid for values of S_w greater than 10%, while the constant value $\sigma_t = 21$ [MPa] is considered for values lower than 10%.
The influence of the mechanical damage on the mortar permeability is supported by more recent experiments [9, 10]. In particular, the water vapour diffusion C_h^v and the liquid water diffusion C_h^l, which define the mortar permeability $C_h = C_h^v + C_h^l$, are scaled by two factors g_d^v and g_d^l, respectively, which both depend on the percentage of damaged mortar area $\beta = \alpha \big/ (1 + \alpha)$, according to the following laws:

$$g_d^v = -1.875\beta^2 + 1.5\beta + 1\,, \quad g_d^l = 1 + (b_1\beta)^{b_2} + 1/2(b_1\beta)^{2b_2} + 1/6(b_1\beta)^{3b_2} \tag{13}$$

where $b_1 = 11.3$ and $b_2 = 1.64$ are the coefficient values tuned on concrete materials.

3.2 Effects of moisture rising on the structural response

The structural response and carrying capacity are determined by performing push-over like analysis: once humidity diffusion gets the steady-state and preliminary gravity loading are applied, shear loading are monotonically increased according to an amplification

factor, up to the ultimate condition of the structure. The equilibrium path during this varying loading condition is recovered in terms of such an amplification factor and the average lateral displacement of the wall.
Figure 4 reports the equilibrium paths followed by the two tested walls, so as to compare structural performance in dry conditions with respect to those in wet conditions, for both the walls. Such wet conditions are attained by conducting a diffusive analysis as we will describe in the next Section. Both structural responses highlight how the presence of humidity rising on the wall significantly affect the pre- and post-critical mechanical behaviours. Less evident is the influence of different diffusive conditions when the ultimate shear load is attained. Such conditions indeed affect only the softening response of the stress according to how the damage can diversely evolve and distribute; the limit load is instead characterized almost by the friction toughness which is predominant on the structural response as the damage becomes greater and greater.

By comparing the equilibrium paths in Figure 4, the two-storey wall is more sensitive than the three-store wall to the different damage distributions passing from dry to wet case. This result can be explained by considering that the shear limit conditions are expected to be more evident in lower than higher walls.
In order to clarify this point two-by-two snapshots of damage maps over the structure are reported in Figures 6 and 7. Dry and wet cases have quite similar spatial distribution over the two walls. However, damage can grow along the left side more significantly in the three-storey wall compared to that of the two-storey wall, since the former wall is subject to a mechanical behaviour more flexural than shear, with respect to the latter wall.

3.3 Effects of damage level on moisture rising

The humidity diffusion analysis is conducted by simulating moisture rising from ground, with evaporating conditions either applied as boundary Neumann conditions on all the external surfaces, and applied in the entire wall domain as source term.
As the curves of volumetric water uptake show (see Figure 5), the presence of a damage pattern increases noticeably the water content evolving in time. For both the walls, such curves describe a qualitatively similar increment at steady-state conditions, as expected by the fact that the moisture rising is imposed from the ground of both the walls, and the damage pattern is mostly concentrated in the lower parts. However, the increment of the volumetric water content in the lowest wall doesn't exceed a value of 8%, while in the highest wall it attains about a 20%. This result can be explained in reason of a wider distribution of both damage and humidity in the three-storey wall, for the same inflow surface area at the ground.

The differences in humidity distribution over the walls are also emphasized in Figures 6 and 7. Due to the different mechanical conditions (undamaged versus damaged wall), the humidity significantly rises up to the first floor in the initially damaged wall for both the analyzed cases. In particular, both the walls are characterized by a very similar moisture rising in the undamaged cases (see figures on the left), owing to the identical boundary

conditions imposed in the diffusion problems. However, the damage distribution in the three-storey wall, which has a more pronounced flexural response with respect to the two-storey wall, leads the moisture rising to assume a more evident straight front, while the steady-state front attained in the two-storey wall follows more evidently diagonal, shear-like, lines.

REFERENCES

[1] Formica G, Sansalone V, Casciaro R. A mixed solution strategy for the non linear analysis of brick masonry walls. *Comput Method Appl M* (2002) **191**:5847–5876.

[2] Castellazzi G, de Miranda S, Formica G, Molari L, Ubertini F. Coupled hygro-mechanical multiscale analysis of masonry walls. *Eng Struct* (2015) **84**:266–278.

[3] Castellazzi G, Colla C, de Miranda S, Formica G, Gabrielli E, Molari L, Ubertini F. A coupled multiphase model for hygrothermal analysis of masonry structures and prediction of stress induced by salt crystalization. *Constr Build Mater* (2013) **41**:717–731.

[4] Brasile S, Casciaro R, Formica G. Multilevel approach for brick masonry walls - Part II: On the use of equivalent continua. *Comput Method Appl M* (2007) **196**:4801–4810.

[5] Brasile S, Casciaro R, Formica G. Multilevel approach for brick masonry walls - Part I: A numerical strategy for the nonlinear analysis. *Comput Method Appl M* (2007) **196**:4934–4951.

[6] Jansen KE, Whiting CH, Hulbert GM. A generalized-α method for integrating the filtered Navier-Stokes equations with a stabilized finite element method. *Comput Method Appl M* (2000) **190**:305–319.

[7] Sykora J, Krejci T, Sejnoha M. Computational homogenization of non-stationary transport processes in masonry structures. *J Comput Appl Math* (2012) **236**: 4745–4755.

[8] Glucklich J, Korin U. Effect of Moisture Content on the strength and strain energy release rate of cement mortar. *J Am Ceram Soc* (1975) **58**:517–521.

[9] Pijaudier-Cabot G, Dufour F, Choinska M. Permeability due to the increase of damage in concrete: from diffuse to localized damage distribution. *J Eng Mech-ASCE* (2009) **135**:1022–1028.

[10] Rouchier S, Foray G, Woloszyn M, Roux JJ. Influence of diffuse damage on the water vapour permeability of fibre reinforced mortar. *Transport Porous Med* (2012) **93**:543-559.

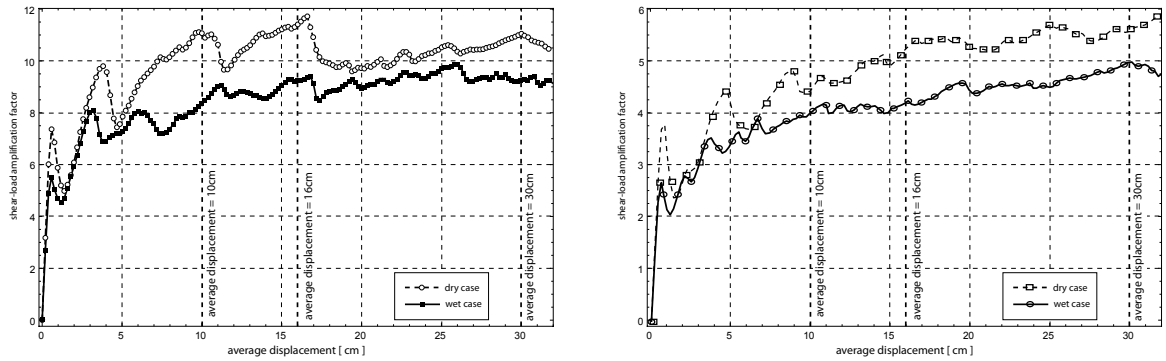

Figure 4: Structural responses in the presence of moisture (wet case) compared with the dry case: two-storey wall on the left, three-storey wall on the right.

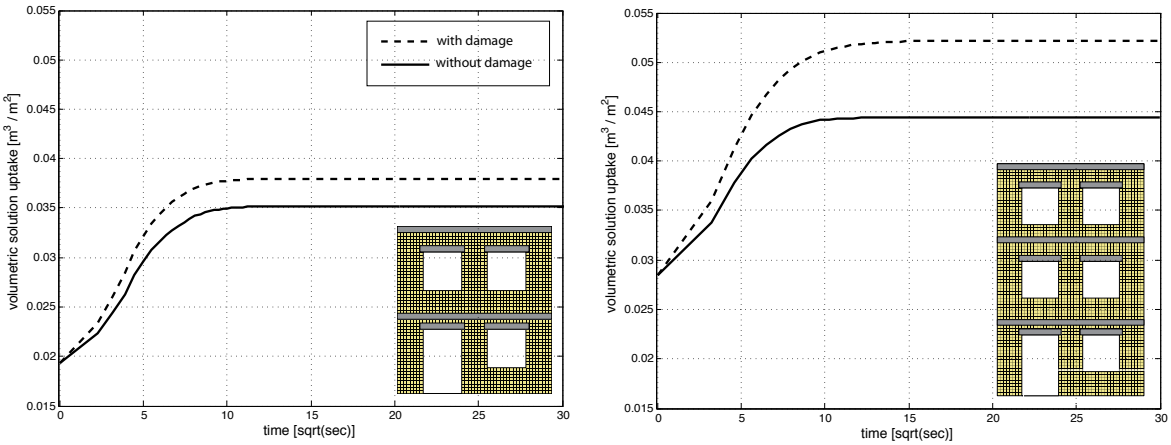

Figure 5: Volumetric water uptake with and without initial damage: two-storey wall on the left, three-storey wall on the right.

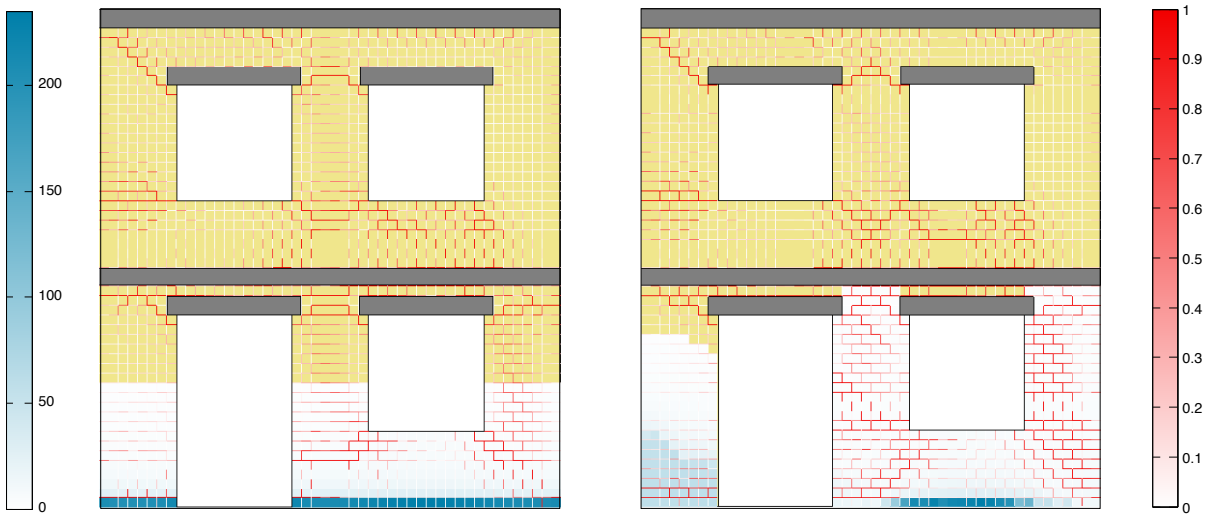

Figure 6: Two-storey wall: damage and water content distributions. Damage in dry conditions on the left, in wet conditions on the right; water content in undamaged conditions on the left, in damaged conditions on the right.

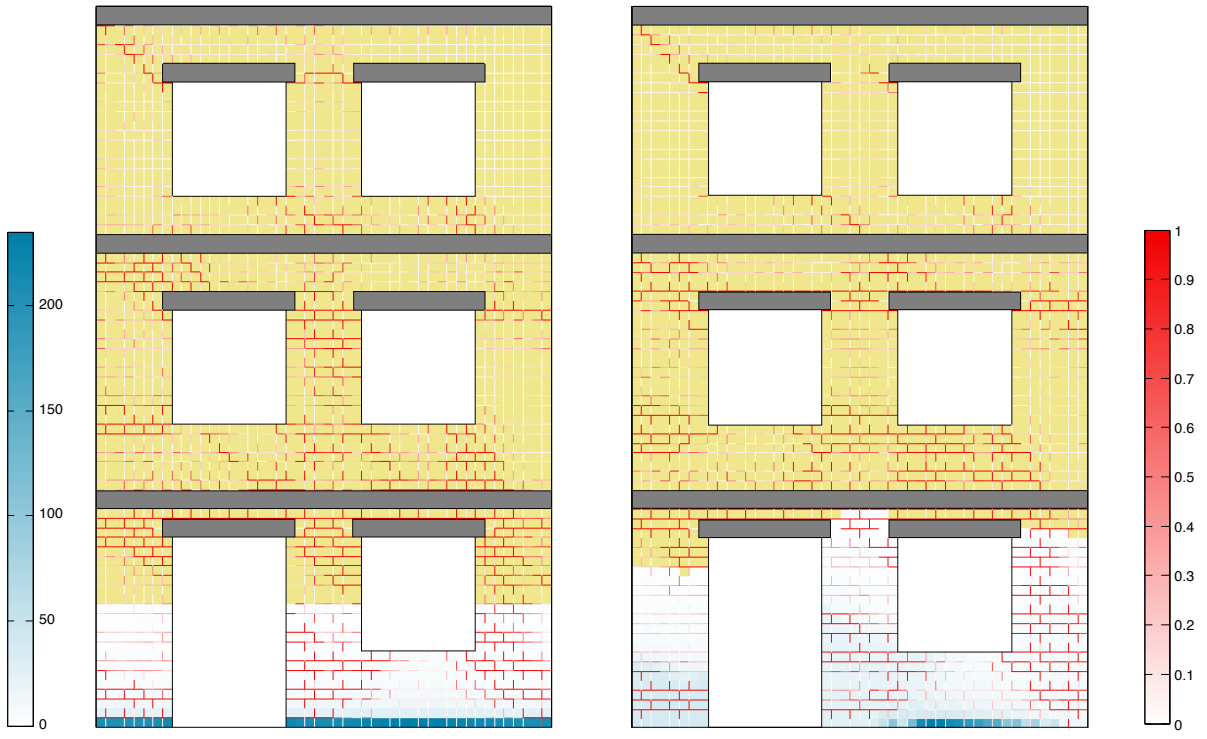

Figure 7: Three-storey wall: damage and water content distributions. Damage in dry conditions on the left, in wet conditions on the right; water content in undamaged conditions on the left, in damaged conditions on the right.